Radiation force in the magneto-optical trap

A. M. Steane, M. Chowdhury, and C. J. Foot

Clarendon Laboratory, Oxford University, Oxford, England

Received November 6, 1991; revised manuscript received June 1, 1992

An overview of the theory of the magneto-optical trap is presented, along with measurements of the effect of an imbalance in the intensities of the trapping beams. This investigation tests the theory of the spring constant of the trap and confirms that the confining force at the center of the trap results from an induced orientation of the atomic ground state. The experimental results give the magnitude of this force, which has not yet been calculated accurately. We calculate the radiation field in the three-dimensional molasses, finding that the relative time phase of the orthogonal standing waves is significant, and we give some insight into the phenomenon of interference fringes when the beams are misaligned. We also discuss the limitation of the trapped atomic density resulting from photon scattering within the cloud, predicting that densities above 10^{13} atoms/cm^3 could be achieved in a trap operating at low saturation of the atomic transition. Finally, we briefly consider collisional loss at low densities, finding an especially large contribution from resonant dipole–dipole scattering.

1. INTRODUCTION

The magneto-optical trap was first experimentally realized by Raab *et al.*[1] in 1987 and has since become almost a standard technique for obtaining large numbers of cold atoms. Experiments have used such a trap merely as a source of cold atoms or have investigated the properties of the trap itself. This paper is a contribution to the latter task and brings together a number of results concerning the radiation force in the trap and the properties of the cloud of trapped atoms. The radiation force in the magneto-optical trap was first described[1] simply in terms of photon scattering (Doppler theory) without regard to the significance of polarization gradients in the radiation field. However, once the role of such gradients in optical molasses was recognized,[2] it soon became apparent that one must take them into account in understanding the magneto-optical trap also.[3] As yet, no summary of the sub-Doppler theory of the trap has appeared, so such a summary is provided here in Section 4. Most of the results are simply a small adaptation of the theory of optical molasses. However, we provide some new physical insights and discuss the possibility of obtaining higher densities of atoms in the trap than have been seen so far.

Section 2 introduces the basic concepts involved in understanding the trap. Loading the trap from an atomic vapor is described, and the cross section for loss by collisions with fast background atoms is calculated. The calculation shows that the loss is significantly increased when the background consists of atoms of the trapped species because of the resonant dipole–dipole interaction. Section 3 then considers the maximum density of trapped atoms that can be obtained. The theory of Sesko *et al.*[4] is reproduced by a simple calculation, and we give an estimate of the variation of the limiting density with laser detuning and intensity. This estimate can be used once one has an expression for the spring constant of the trap. Section 4 provides such an expression, which is valid in the case of low intensity, along with a discussion of other features of the radiation force. We consider the radiation field consisting of three orthogonal standing waves, and we point out that the friction parameter can be expected to vary dramatically with the relative phase of one standing wave with respect to the others, a result similar to that recently noted by Molmer[5] for a two-dimensional molasses. This analysis also gives some insight into the channeling of atoms in interference fringes when the beams are misaligned.

We reported an initial experimental verification of some of this theory in our previous study.[3] More-accurate experiments are described in the later sections of the present paper.

2. BASIC CONCEPTS

Atoms in a trap are subject to a force that is a complicated function of position and velocity. The force can vary significantly over distances of the order of a wavelength (~ 1 μm), while atoms confined in the trap move about over distances of the order of ~ 1 mm. During this motion the small-scale variations in the force are averaged, so that in a first approach to modeling the behavior one uses a force $\mathbf{f}$ that is equal to the actual force averaged over time and over one or several wavelengths. At velocities for which the Doppler shift equals the light shift, or for positions toward the edge of the trapping region, $\mathbf{f}$ is not a linear function of velocity or position. However, once atoms are captured, they are typically slowed to low velocities and confined close to the center of the trap, so that the components of $\mathbf{f}$ may be written as

$$f_i(\mathbf{r},\mathbf{v}) = -\sum_j \kappa_{ij} r_j - \sum_j \alpha_{ij} v_j \qquad \text{for small } r, v. \tag{1}$$

Thus κ_{ij} is a spring tensor, and α_{ij} is a friction tensor. The (rapid) random fluctuations in the force may be modeled by a diffusion constant D, so that a cloud of atoms in the trap will have an equilibrium temperature determined by the Fokker–Planck equation.[6] The steady-state solution to the Fokker–Planck equation for a damped one-dimensional harmonic oscillator gives

$$k_B T = D_1/\alpha. \tag{2}$$

0740-3224/92/122142-17$05.00

This is the same as the result obtained for optical molasses—the temperature is not affected by the conservative part of the force. The one-dimensional diffusion constant D_1 is equal to one component of the diffusion tensor that appears in the three-dimensional Fokker–Planck equation; $D_1 = D/3$ in a spherically symmetric case.

The first experiment[1] with a magneto-optical trap measured the parameters κ and α along with various other properties. The values were compared with a calculation based on the scattering force and showed reasonable agreement. Further calculations[7] of the confining force in two dimensions have continued to use a simple scattering-force argument. Our earlier study[3] and the present discussion show, however, that polarization-gradient forces are present and lead to markedly different values for κ, α, and T.

The other parameters of interest, from the point of view of using the trap as a source of cold atoms, are as follows:

Number of atoms in the trap	N,
Number density of atoms	n,
Lifetime for an atom to remain in the trap	τ,
Maximum velocity for an atom to be captured by the trap	v_c,
Escape velocity for an atom in the center of the trap	v_{esc}. (3)

The parameters v_c and v_{esc} are averaged, rather than exactly defined, quantities, since the velocities depend on the trajectory of an atom entering or leaving the trap. v_c and v_{esc} are of the same order of magnitude, but it is useful to distinguish between them in order to emphasize the difference between the trajectories involved: A captured atom approaches the trap with a comparatively large velocity at the edge of the trap and is slowed as it approaches the trap center, while an escaping atom has a large velocity at the center of the trap and is slowed as it leaves.

All our quoted values are for the cesium atom and the $6S_{1/2}F = 4 \rightarrow 6P_{3/2}F = 5$ transition, unless otherwise indicated. Thus the atomic mass $m = 2.21 \times 10^{-25}$ kg, the transition linewidth (FWHM) is $\Gamma = 2\pi \times 5.3$ MHz, and the saturation intensity (of the $M = 4 \rightarrow M = 5$ component) is $I_S = 2.25$ mW/cm^2, defined according to the convention $I/I_S = (\Omega/\Gamma)^2$, where Ω is the Rabi frequency. The saturation parameter is

$$s = \frac{\Omega^2/2}{\delta^2 + \Gamma^2/4}. \tag{4}$$

A. Loading

The number of atoms in the trap is determined by a balance between the capture rate R into the trap and the loss rate from the trap. This relationship gives the rate equation

$$\frac{dN}{dt} = R - \frac{N}{\tau} - \beta\frac{N^2}{V}. \tag{5}$$

The third term on the right-hand side represents loss resulting from two-body collisions between atoms in the trap, which are significant at high densities of trapped atoms.[8] (The volume $V = N/n$ is included so that the definition of β agrees with that in Ref. 8, where its size is found to be of the order of 10^{-11} cm^3/s for cesium, depending on the laser parameters.) When the loading and loss rates are independent of N (i.e., the β term is insignificant), one has the solution

$$N(t) = [N(0) - R\tau]\exp(-t/\tau) + R\tau. \tag{6}$$

The loading rate R depends on the method used to load the trap. τ is usually determined by collisions, i.e., events in which atoms in the background gas knock atoms out of the trap.

The simplest loading method is to form a trap in a low-pressure vapor of atoms of the species to be trapped. An approximate model for the loading is that the trap catches all atoms that enter the trapping region with a velocity less than the maximum capture velocity v_c. The kinetic theory of gases is used to calculate the flux of such atoms, yielding the formula (cf. Ref. 9)

$$N = R\tau \simeq \frac{1}{5}\left(\frac{v_c}{\bar{v}}\right)^4 \frac{A}{\sigma}, \tag{7}$$

where $\bar{v} = (8k_B T/\pi m)^{1/2}$ is the average speed in the background vapor, A is the surface area of the trapping region, and σ is the cross section for trap loss by collisions with atoms in the background vapor (assumed to be the dominant loss mechanism). The numerical factor depends somewhat on the method used to define A—a more accurate theory would take account of the fact that the maximum capture velocity will depend on the trajectory of an atom approaching the trap. The loading rate rises rapidly with the capture velocity v_c. The capture velocity itself depends on the size of the trap (being larger for larger trapping volumes), so that N increases quite rapidly as the radius of the trapping region increases. A typical value for v_c is the velocity of an atom that is stopped in a distance equal to the radius of the trap by a force equal to half the maximum scattering force, i.e., $v_c = (2ar)^{1/2}$, with $a = \hbar k\Gamma/4m \simeq 29{,}300$ m/s^2. For $r = 4$ mm this formula gives $v_c \simeq 15$ m/s (for cesium). (This argument is a slight improvement on the rough value quoted in Ref. 9 and elsewhere, in which the capture velocity is assumed to be limited by the Doppler width of the atomic transition. In fact this limit does not apply, as can be deduced from a simple examination of velocity damping by the scattering force in a laser standing wave. The force is still significant at velocities above a few Doppler widths, especially when the laser is detuned a linewidth or two; cf. Ref. 10.)

The number of atoms in the trap is independent of the density of the background gas and therefore of the pressure in the vapor cell. This assertion will be valid except at low vapor pressures, when other atomic species form a significant fraction of the background gas. Also, the number density at the center of the trap is reduced if the time taken for incoming atoms to reach the center is comparable with the lifetime in the trap. Using $\sigma = 20 \times 10^{-14}$ cm^2 (see Subsection 2.B), a trap radius of 4 mm, and $v_c = 15$ m/s, one obtains, at room temperature, $N = 1.2 \times 10^7$. This gives the order of magnitude of the number obtained experimentally.[9]

B. Collisional Loss

An interatomic collision is dominated at long ranges by the lowest-order nonzero term in the molecular potential.

Table 1. Estimates of Cross Section σ from Measurements of Lifetime τ

Trapped Species	Background Species	σ (10^{-14} cm^2)	Reference
Na	N_2	3.3	12
Na	Na	~100	13
Cs	He	~6	14
Cs	Cs	20	9

For two ground-state atoms, this is usually the van der Waals interaction, which is an attractive C_6/R^6 potential (R is the interatomic separation). For a collision between a ground-state atom and an excited-state atom there is a longer-range resonant dipole–dipole interaction of the form[11]

$$\frac{C_3}{R^3} = \frac{|d|^2}{4\pi\epsilon_0 R^3} \tag{8}$$

$$\Rightarrow C_3 = \frac{3}{4}\left(\frac{\lambda}{2\pi}\right)^3 \hbar\Gamma \tag{9}$$

$$= 6.56 \times 10^{-48}\,\mathrm{Jm}^3 \qquad \text{for cesium}, \tag{10}$$

where d is the electric dipole matrix element. This interaction shifts the levels by one linewidth when the atoms are separated by approximately one wavelength.

Traps for neutral atoms typically have depths of less than 1 K while residing in an evacuated chamber whose walls are at room temperature. Therefore atoms of the background gas in the chamber can easily knock atoms out of the trap. From the kinetic theory of gases, the rate of collisions between background atoms and atoms in the trap is $N/\tau = (N\sigma)(n_b\bar{v})$, where n_b is the density of background atoms and $\bar{v}$ is the mean relative velocity of the colliding atoms, i.e., the mean velocity of the background atoms, since those in the trap are approximately stationary. For a background gas at temperature T and pressure P we have $n_b = P/k_BT$ and $\bar{v} = (8k_BT/\pi m)^{1/2}$; therefore

$$\tau = \frac{(\pi m k_B T/8)^{1/2}}{\sigma P}. \tag{11}$$

Measurements of the lifetime τ in a magneto-optical trap have been used to estimate the cross section σ, with results as listed in Table 1. For example, in a background of cesium at room temperature and a pressure of 10^{-8} Torr, one obtains $\tau \simeq 1$ s. There is some indication in these results that atoms in the trap interact more strongly with atoms of the same species than with atoms of other species, as was remarked by Cable *et al.*[13]

An independent measurement of the van der Waals interaction between ground-state cesium atoms gives $C_6 = 6.95 \times 10^{-76}$ Jm^6 (Table 1 of Ref. 15). The total cross section in the classical limit (many partial waves), as given by Massey (p. 1324 of Ref. 16), is

$$\sigma = f(n)(C_n/\hbar v)^{2/n-1}, \tag{12}$$

where $f(3) = 20.2$ and $f(6) = 8.08$; Eq. (12) then gives (for the van der Waals interaction) $\sigma = 30 \times 10^{-14}$ cm^2, for $v = 220$ m/s (mean velocity at room temperature). The trapped atoms can spend a significant proportion of the time in the excited state. Using Eqs. (12) and (9), we obtain $\sigma = 5700 \times 10^{-14}$ cm^2 for the resonant dipole–dipole interaction. Thus, if a proportion P of the collisions involve an excited atom, we expect a total cross section of $\sim[5700P + 30(1 - P)] \times 10^{-14}$ cm^2. A typical value is $P = 0.3$, giving $\sigma \simeq 1700 \times 10^{-14}$ cm^2. The measured value is much smaller than this, since not all collisions that contribute to the theoretical total cross section will dislodge an atom from the trap and thus contribute to the cross section for trap loss.

We can estimate the expected cross section for knocking atoms out of the trap as follows. The collision time is much smaller than the time scale of motion in the trap, so that the displaced atom can be regarded as instantaneously acquiring a finite velocity. The atom will leave the trap if this velocity is greater than the escape velocity v_{esc}. We will calculate the impact parameter b for a collision that exerts an impulse $\Delta p = mv_{esc}$ on the trapped atom; the cross section for knocking atoms out of the trap will then be $\sigma = \pi b^2$. If v_{esc} is much less than a typical velocity for an atom in the background gas, then the incident atom is hardly affected by the collision, and we may regard it as moving at constant velocity along a straight line past the trapped atom (see Fig. 1 and Ref. 17). The total impulse is

$$\Delta\mathbf{p} = \int_{-\infty}^{\infty} \mathbf{F}\,\mathrm{d}t, \tag{13}$$

where

$$F = \frac{nC_n}{R^{n+1}}, \qquad R = \frac{b}{\cos\theta}, \qquad \tan\theta = \frac{vt}{b}. \tag{14}$$

The component of $\mathbf{F}$ in the direction parallel to the trajectory of the fast atom averages to zero, and the other component, $F\cos\theta$, is integrated as follows:

$$\Delta p = \int_{-\pi/2}^{\pi/2} \frac{nC_n}{vb^n}(\cos^n\theta)\mathrm{d}\theta \tag{15}$$

$$= f(n)\frac{C_n}{vb^n} \qquad \left[f(3) = 4, \quad f(6) = \frac{15\pi}{8}\right] \tag{16}$$

$$\Rightarrow \sigma = \pi\left(\frac{f(n)C_n}{mv_{esc}v}\right)^{2/n}. \tag{17}$$

A typical value is $v_{esc} \sim 15$ m/s (see Subsection 2.A). Inserting this value into our equation for σ, with $v = 220$ m/s, gives $\sigma = 5.6 \times 10^{-14}$ cm^2 and $\sigma = 34 \times 10^{-14}$ cm^2 for the van der Waals and resonant dipole–dipole interactions, respectively. The latter result agrees with the measured value, while the former shows that for two ground-state atoms the cross section is only a few times

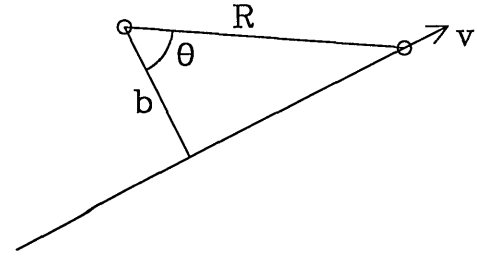

Fig. 1. Geometry of a collision in which the fast atom is almost unperturbed.

larger than that for a close approach of the atoms (a hard-sphere collision). Using a diameter of 0.6 nm for the cesium atom gives a hard-sphere cross section of $\sim 1 \times 10^{-14}$ cm^2.

The argument of the present section implies that the trap lifetime will vary significantly with the proportion of trapped atoms in the excited state if the background gas consists largely of atoms of the trapped species. This effect would reveal itself as a dependence of the lifetime on the saturation parameter of the trapping light. The escape velocity also depends on the light intensity and detuning, so that the expected trap lifetime can be calculated only once one has a detailed model for the capture process.

3. PHOTON PRESSURE AND LIMITING ATOMIC DENSITY

The density of trapped atoms is limited by two factors. First, the thermal motion of atoms in the trap causes them to spread out to an rms radius given by the equipartition theorem:

$$\tfrac{1}{2} k_B T_i = \tfrac{1}{2} \kappa_{ii} \langle r_i^2 \rangle. \tag{18}$$

The solution of the Fokker–Planck equation for a damped simple harmonic oscillator gives a Gaussian density distribution. As more atoms are loaded into the trap at a given equilibrium temperature, the size of the cloud stays constant while the density increases. Eventually, the increase in density is limited by repulsive forces between the atoms. The density is then determined by the relative magnitude of the repulsive forces and the spring constant of the trap. In this section we consider the net repulsive force resulting from the scattering of photons from one atom to another in the trap.[4,18] The description given by Sesko *et al.*[4] can be reproduced in an intuitively obvious way as follows. Consider two atoms separated by a distance r in a laser field of saturation parameter s [Eq. (4)]. Here s is the total saturation parameter, though below we use it to refer to the saturation parameter per laser beam. The rate at which one atom scatters photons from the laser is $\Gamma s/2(s+1)$. If the cross section for the other atom to absorb these reradiated photons is σ_R, then there is a photon-pressure force between the atoms equal to

$$\mathbf{F}_R = \frac{\hbar k \Gamma}{2} \frac{s}{(s+1)} \frac{\sigma_R}{4\pi r^2} \hat{\mathbf{r}} \tag{19}$$

$$= \frac{I \sigma_L}{c} \frac{\sigma_R}{4\pi r^2} \hat{\mathbf{r}}, \tag{20}$$

where

$$\sigma_L = \frac{\hbar \omega_L \Gamma}{2} \frac{s}{I(s+1)} \tag{21}$$

$$= \text{the cross section for absorption of photons from the laser field.} \tag{22}$$

We have assumed isotropic radiation and unpolarized atoms for simplicity. Also, the photon-pressure force is calculated for a two-level atom. The force satisfies an inverse-square law, so that we may use Gauss's theorem to derive the divergence of the force in a cloud of atomic density n: $\nabla \cdot \mathbf{F}_R = \sigma_L \sigma_R I n/c$ (cf. Maxwell's equation, $\nabla \cdot \mathbf{E} = \rho/\epsilon$). Strictly speaking, $\mathbf{F}_R$ arises from part of the total force between the radiation and the atoms. However, it is helpful to think of it as a repulsive force between the atoms. Another contribution can be imagined to be an attractive force between the atoms, arising because atoms at the side of the cloud will attenuate the incoming laser beams, producing an intensity imbalance that tends to compress the cloud. This force can be expressed by analogy with the repulsive force by considering that each atom casts a shadow in the laser field of area σ_L; thus

$$\mathbf{F}_A = -\frac{I {\sigma_L}^2}{c 4\pi r^2} \hat{\mathbf{r}}. \tag{23}$$

An initial paper on these effects[19] failed to consider the repulsive contribution to the force and so concluded that there is increased compression of the trapped gas. However, an experimental investigation[18] showed that the repulsive force is larger than the attractive force for typical parameter values in a magneto-optical trap, so that the photon scattering limits the density of the trapped cloud. The trapped cloud adopts a density distribution such that the scattering within the cloud just balances the trapping force $-\kappa r$ (we assume spherical symmetry for simplicity). For an inverse-square-law force, the net force at radius r that is due to a spherical distribution of atoms is equal to that produced by N atoms at the origin, where N is the number of atoms within the radius r. This means that the density distribution that balances the trapping force is simply a uniform distribution of density n, given by

$$\kappa r = \frac{4}{3} \pi r^3 n \frac{I {\sigma_L}^2 (\sigma_R/\sigma_L - 1)}{c 4\pi r^2} \tag{24}$$

$$\Rightarrow n = \frac{3\kappa c}{I {\sigma_L}^2 (\sigma_R/\sigma_L - 1)}. \tag{25}$$

If we obtain κ from a model of the trap, then the only unknown parameter is $\sigma_R/\sigma_L - 1$. This parameter can be different from zero because the reradiated light can have a spectral distribution that is different from that of the laser light. The spectral distribution of the reradiated light consists of two parts,[20] the elastic (Rayleigh scattering) contribution and the inelastic (fluorescence). The elastically scattered light has the same spectral distribution as the laser light, while the inelastic scattering has the familiar Lorentzian form at low laser intensities, tending to the Mollow[21] triplet form at high intensities. To calculate the absorption cross section for the reradiated light, one must derive the cross section for absorption of light at one frequency in the presence of intense light of another (near-resonant) frequency.[22] An accurate calculation is thus somewhat complicated. However, one may obtain an approximate value for σ_R/σ_L as follows. Mollow [Eq. (3.24) of Ref. 21] gives the intensity of the elastically scattered light as a fraction of the total scattered intensity:

$$\frac{I_{\text{el}}}{I_{\text{el}} + I_{\text{inel}}} = \frac{1}{s+1}. \tag{26}$$

The absorption cross section for the elastically scattered light will be the same as that for absorption of the laser

light. The inelastic light, however, has a larger absorption cross section, since the absorption coefficient in the presence of the laser field is peaked near the Mollow triplet components (especially the blue-shifted component, which lies close to the atomic resonance at high laser detunings). We may estimate the cross section for absorption of the inelastically scattered light by writing it as equal to the cross section for absorption of the laser light when the laser is at zero detuning. The argument here is that the modified absorption coefficient has peaks with widths similar to the natural linewidth of the transition, so that the cross section for absorption of light at the peak absorption frequency is similar to the usual absorption cross section at resonance. Thus, if σ_L is the cross section for absorption of laser light for laser detuning δ, then that for absorption of the inelastic light is roughly

$$\frac{\delta^2 + \Gamma^2/4 + \Omega^2/2}{\Gamma^2/4 + \Omega^2/2}\sigma_L = \frac{s+1}{s + \Gamma^2/(4\delta^2 + \Gamma^2)}\sigma_L. \tag{27}$$

Combining the two contributions to the scattered light in the ratio indicated by Eq. (26), we obtain

$$\sigma_R \simeq \frac{1}{s+1}\sigma_L + \left(1 - \frac{1}{s+1}\right)\frac{s+1}{s + \Gamma^2/(4\delta^2 + \Gamma^2)}\sigma_L \tag{28}$$

$$\Rightarrow \frac{\sigma_R}{\sigma_L} - 1 \simeq \left(\frac{s}{s+1}\right)\frac{\delta^2}{s(\delta^2 + \Gamma^2/4) + \Gamma^2/4}. \tag{29}$$

For cesium at $I = 12$ mW/cm^2 and $\delta = 1.5\Gamma$, Walker *et al.*[18] obtained $\sigma_R/\sigma_L - 1 = 0.2$ by a more careful numerical calculation (convolving the emitted spectrum with the modified absorption coefficient). For this case $s = 1.07$, and our relation (29) gives $\sigma_R/\sigma_L - 1 = 0.4$. Thus both calculations reproduce Walker's experimental value of 0.3 as well as can be expected for such a simplified theory. We emphasize that our method of calculation is approximate and is probably less accurate than that of Ref. 18. The advantage of relation (29) is that it is derived analytically, and it indicates roughly how the cross section ratio will vary with laser intensity and detuning. Our estimate of the scattering cross sections is for a two-level atom, whereas below we deduce the spring constant of the trap while allowing for the multiple Zeeman sublevels of the atomic ground state. The next stage would be to allow for this multilevel structure throughout the calculation, which is outside the scope of this paper. At low intensities $\sigma_R \simeq \sigma_L$, so the limiting density [Eq. (25)] is sensitive to a delicate balance between attractive and repulsive forces. This implies that a completely multilevel calculation might yield a result significantly different from relation (29) in this regime. An experimental investigation of this regime would be worthwhile.

4. DAMPING AND RESTORING FORCES

We now turn to the calculation of the radiation force in the magneto-optical trap (at low atomic density), concentrating on the region near the center of the trap, for low velocities, where Eq. (1) can be used. The wavelength-averaged parameters κ and α are then independent of velocity and position, and one has damped simple harmonic motion. The equation of motion $f = m\mathrm{d}v/\mathrm{d}t$ is solved with

$$z = \exp\left(-\frac{\alpha}{2m}t\right)\left[A\exp\left(\frac{\beta}{2m}t\right) + B\exp\left(-\frac{\beta}{2m}t\right)\right], \tag{30}$$

where

$$\beta = (\alpha^2 - 4m\kappa)^{1/2}, \tag{31}$$

$$\frac{A}{B} = \frac{\beta + \alpha}{\beta - \alpha} \tag{32}$$

for boundary condition $\mathrm{d}z/\mathrm{d}t = 0$ at $t = 0$. The motion consists of damped oscillations when β is imaginary or exponential decay to the origin when β is real. The transition between the two types of motion occurs for critical damping,

$$\beta = 0 \Rightarrow \kappa/\alpha = \alpha/4m. \tag{33}$$

In practice the motion is almost always overdamped. This result is expected, once polarization gradient forces are taken into account, as we show below. In the overdamped case it is noteworthy that the motion of the atoms is largely independent of their mass. For $\alpha^2 \gg 4m\kappa$ the solution to the equation of motion satisfying $\mathrm{d}x/\mathrm{d}t = 0$ at $t = 0$ has $A/B \simeq \alpha^2/m\kappa \gg 1$. Therefore only the A term is significant, and one has exponential decay with a time constant

$$\frac{2m}{\alpha - \beta} \simeq \frac{\alpha}{\kappa}\left(1 - \frac{m\kappa}{\alpha^2} + \ldots\right). \tag{34}$$

In this regime an atom moving toward the trap center is surfing on the force curve; that is, the radiation force damps the atomic velocity toward a finite velocity that decreases as the atom approaches the trap center (cf. Zeeman slowing of an atomic beam[23]).

The lowest temperatures in three-dimensional optical molasses are obtained in the laboratory only once the residual magnetic field in the apparatus is canceled, because the sub-Doppler cooling mechanisms rely on the differing light shifts of the magnetic sublevels and on optical pumping among them. It is important that Zeeman shifts and Larmor precession do not exceed the light shifts or interfere with the optical pumping. For this reason it was assumed that polarization gradient forces would not be significant in the magneto-optical trap, since the trapping potential relies on the magnetic field. However, a careful experimental survey of optical molasses, using sodium,[24] showed that a temperature half of the Doppler cooling limit is obtained in a magnetic field of 1 G. (At 1 G the Larmor precession frequency is of the same order of magnitude as the optical pumping rate.) As we show below, the cloud in a magneto-optical trap can easily be confined to a region in which the magnetic field is everywhere less than 0.05 G, so that sub-Doppler cooling is expected. This affects the predictions for compression of an atomic beam using a two-dimensional trap also.[7,25] In Subsection 4.A we summarize our approach to considering the effects of polarization-gradient forces in the

trap, and then we proceed to quote various results, making comparisons with the simple Doppler theory that takes account only of the scattering force.

A. Summary of the Argument

In a one-dimensional standing wave three physical mechanisms have been identified that give rise to a radiation force associated with a gradient of polarization. The first two are the induced-orientation effect in the σ^+–σ^- configuration (opposed beams of σ^+ and σ^- polarization) and the Sisyphus effect in the lin ⊥ lin configuration (that with orthogonal linear polarization).[26] The σ^+—σ^+ configuration with a weak transverse magnetic field also produces a Sisyphus effect.[27] With a stronger magnetic field, however, a third physical process may be identified in the form of a velocity-sensitive magnetic resonance.[28] Which of these processes will be relevant to the magneto-optical trap? If one were to construct a one-dimensional trap, one could isolate one physical mechanism at a time, depending on the choice of laser polarization. In the three-dimensional trap one needs first to examine in detail the polarization state of the radiation field (see Subsection 4.B). In general, more than one type of polarization gradient can be obtained, so that one has a mixture of the physical mechanisms; exact predictions would have to rely on the result of numerical calculations. However, the mixture can be sorted out to some extent as follows.

First we note that the force for a damped harmonic oscillator is equivalent to a purely frictional force that damps the velocity toward a finite velocity whose value depends on position, that is

$$-\alpha v - \kappa z = -\alpha[v - v^{(z)}], \tag{35}$$

where

$$v^{(z)} = -(\kappa/\alpha)z. \tag{36}$$

Now, the σ^+–σ^+ configuration damps the atomic velocity toward a nonzero value only when the Larmor precession frequency is larger than the optical pumping rate, i.e.,

$$g\mu_B B > \hbar\Gamma s, \tag{37}$$

as may be seen by inspecting the calculated force curve in Ref. 28. It is reasonable to argue that this is a general feature of this type of force (e.g., see the further experimental data in Ref. 29). The trap may therefore be divided into two regions, the central low-field region, where the "velocity-selective magnetic resonance"[30] is not significant, and the surrounding high-field region, where it is. Trapped atoms are confined well within the low-field region (see Subsection 4.E), while the high-field region is significant for the capture process.

In the low-field region the only contribution to the position dependence of the force arises from the induced-orientation effect. This gives us our estimate for the spring constant of the trap (Subsection 4.C). In the same low-field region the friction parameter can be expected to be similar to that obtained in optical molasses. There still remains one surprise, however: the type of polarization gradient obtained in the radiation field, and hence the expected size of the force parameters, is sensitive to the relative time phase of one standing wave of the trapping field with respect to the other two (cf. Ref. 31). This dependence should have observable consequences and is discussed in Subsection 4.D.

B. Three-Dimensional Radiation Field

We carried out numerical calculations of the amplitude and polarization of a three-dimensional standing-wave radiation field. The calculation first adds together six electric-field vectors, defined by

$$\mathbf{E}(\mathbf{r})_n = E_n \boldsymbol{\epsilon}_n \exp(i\mathbf{k}_n \cdot \mathbf{r} + \phi_n), \tag{38}$$

where E_n, $\boldsymbol{\epsilon}_n$, and $\mathbf{k}_n$ are the amplitude, polarization vector, and wave vector, respectively, of the nth traveling wave. The directions of the wave vectors are so as to form three perpendicular pairs of opposed beams. We thus obtain the total field amplitude $\mathbf{E}_T(\mathbf{r})$ at any point $\mathbf{r}$. ϕ_n is a phase, which does not depend on position and which is used to examine the dependence of the field on the relative phase of one pair of beams with respect to another. To deduce what type of force one may expect to operate in the trap, it is useful to inspect the state of polarization of the total field as a function of position in the trap. This information is contained in the complex field amplitude $\mathbf{E}_T(\mathbf{r})$. In three dimensions the electric-field vector may rotate about any axis in space, and the polarization may have any degree of ellipticity. It is not easy to depict all this information in graphical form. One can gain insight into the cooling forces, however, by considering a related parameter p, which is defined as follows. We first choose a quantization axis and then calculate the scalar products ξ^+ and ξ^- of the total field with a unit field of σ^+ and σ^- polarization defined for the chosen quantization axis $\mathbf{q}$:

$$\xi^{\pm} = \mathbf{E}_T \cdot [\boldsymbol{\epsilon}^{\pm}_{(\mathbf{q})}]^*. \tag{39}$$

We then define $p = (|\xi^+|^2 - |\xi^-|^2)$. Thus p is proportional to the difference in the light shifts of, and optical pumping rate toward, the ground-state sublevels $M_J = +J$ and $M_J = -J$ for a stationary atom. When p varies between positive and negative values for positions separated by a quarter of a wavelength, one deduces that Sisyphus cooling is present. One can also normalize p by dividing it by the light intensity $\mathbf{E}_T \cdot \mathbf{E}_T^*$. A value of plus or minus one then indicates right- or left-handed circular polarization; a value of zero indicates linear polarization for the chosen quantization axis.

Figure 2 shows graphs of p for some example cases. The calculations show that, to obtain a linear polarization everywhere in the trap, it is necessary to align the beams accurately and also to control the relative phase between one pair of beams and another. It this is not done, then σ^+ and σ^- regions are obtained, so that Sisyphus cooling is expected. The friction and diffusion parameters produced by the Sisyphus effect are larger than those produced by induced orientation by a factor of $\sim(\delta/\Gamma)^2$ at high detunings (see Subsection 4.D), so one expects the friction and diffusion to depend on the relative phase of the standing waves. The same result in two dimensions was pointed out by Molmer.[5]

Our calculations of the radiation field also give some insight into the phenomenon of interference fringes observed in the fluorescence from atoms in a trap or optical molasses. Bigelow and Prentiss[32] showed that the dark

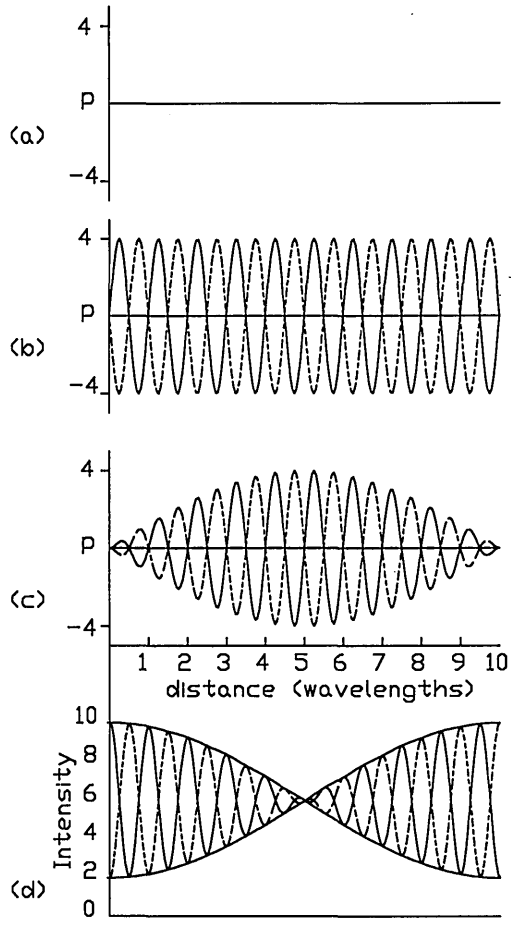

Fig. 2. Presence of Sisyphus cooling in the trap. (a)–(c) show the parameter p defined in the text. The calculation added six plane waves of unit amplitude, each pair having opposite circular polarizations, as for a trap. (a) Aligned beams, all at the same phase angle. (b) Aligned beams, with the x beam pair shifted in phase by $\pi/2$ rad with respect to the others. (c) As in (a) but with the x beams misaligned in the x–y plane, one by +0.05 rad, the other by −0.05 rad. Each graph shows the variation of p along a set of four lines parallel to the y axis (which is also the quantization axis), the lines being separated in the x direction by a quarter of a wavelength. For some cases $p = 0$ is obtained for all y. (d) Intensity for the misaligned-beams case. The wavelength-scale intensity fluctuations occur along the same lines for which circular polarization is present but at different y positions. All the graphs are at $z = 0$. At $z = +0.25$ wavelengths, we still find variations in p similar to those shown in (c), but the intensity in (d) fluctuates between approximately 2 and 10 for all x and y. The wavelength-averaged optical potential has an almost uniform depth throughout the trap.

regions are dark because there are no atoms there rather than because the laser intensity falls to zero. Their discussion uses the idea that the atoms are gathering in optical potential wells. Our calculations show, however, that if one misaligns the laser beams by a small angle θ, while the radiation field does contain variations on the relatively large distance scale of λ/θ, as soon as one averages the depth of the optical potential well over a single-wavelength-sized box the variations all disappear. In other words, there is no significant variation in the average optical potential with a period of λ/θ. Our calculations are consistent, instead, with a picture in which the atoms spend more time in regions separated by λ/θ because the time for diffusion in the molasses varies periodically. That is, some regions of the molasses are stickier than others. The ratio of the diffusion and the friction parameters is roughly independent of the type of polarization gradient[5,26]; hence the diffusion time, which is proportional to α^2/D, is longer when the friction is large (i.e., in the σ^+–σ^- regions). The situation is not quite so simple as this, however. Lett *et al.*[24] discuss the diffusion time when the average kinetic energy of the atoms is of the order of the depth of the optical potential well (pinball), finding that "temporary localization of the atoms in the lattice of a standing-wave potential severely retards their macroscopic diffusion time." Bigelow and Prentiss,[33] on the other hand, point out that the rate of damping of the atomic velocity is much reduced in this case. The depth of the optical potential wells itself depends on the Clebsh–Gordan coefficients, and hence on the populations of the ground-state sublevels and on the field polarization, as well as on the intensity. Finally, we have not examined the effect of vortices in the local radiation pressure force.[31] Vortices also depend on the relative time phase of the beams and may be the true cause of the expelling of atoms from the dark regions of the interference pattern, as was suggested in Ref. 31. To test this hypothesis, it would be interesting to measure whether the atoms gather at positions of zero or $\pi/2$ phase difference between the standing waves (in σ^+–σ^- molasses): There are no vortices at the former positions, but there is higher friction at the latter.

C. Spring Constant

The spring constant in the low-field region [inequality (37)] is due to the induced-orientation effect (a contribution that is due to Doppler theory, i.e., to Zeeman shifts of the transition frequencies, is also present but is negligible at low fields). The presence of a magnetic field is easily introduced into the theory of induced orientation described by Dalibard and Cohen-Tannoudji[26]—the velocity to which atoms are cooled is simply shifted to a velocity v_B, obtained as follows. The perturbing Hamiltonian in the rotating frame, with an external magnetic field B, is $V = -\mu_z B + J_z k v$. The magnetic-moment and angular-momentum operators may be expanded thus:

$$J_z = \sum_M |1M\rangle\langle 1M| M\hbar + \sum_{M'} |2M'\rangle\langle 2M'| M'\hbar, \tag{40}$$

$$\mu_z = -\sum_M |1M\rangle\langle 1M| g_{J_1}\mu_B M - \sum_{M'} |2M'\rangle\langle 2M'| g_{J_2}\mu_B M', \tag{41}$$

where 1 and 2 denote the ground and the excited states. We write these out in full to emphasize that the calculation is valid for any transition scheme. The theory is worked out in the low-intensity limit, where the excited-state populations are negligible. Therefore the excited-state terms in the expressions for J_z and μ_z are not significant, and we have

$$\mu_z = -\sum_M |1M\rangle\langle 1M| g_{J_1}\mu_B M = -g_{J_1}\mu_B J_z. \tag{42}$$

The effect of the magnetic field, therefore, is simply to shift the zero of velocity in the calculation. Instead of cooling toward zero velocity in the laboratory, we have

cooling toward a finite velocity v_B along the laser beams, given by

$$v_B = -g_{J_1}\mu_B B/\hbar k . \tag{43}$$

Note that this velocity is independent of the g_J value of the excited state and of the relative populations of the ground-state sublevels. It is different from the velocity whose Doppler shift would just compensate for the imbalance in the scattering force arising from the Zeeman shift of the ground- and the excited-state sublevels. Indeed, it may be possible to find cases (e.g., $F \rightarrow F - 1$) for which the Zeeman shift of the transition frequency gives a spring constant of opposite sign to that produced by induced orientation in the ground state. An experimental investigation of this case may be interesting, to yield either a Zeeman-shift trap with an induced-orientation hole in the middle or a small induced-orientation trap surrounded by a Zeeman-shift expelling region.

The spring constant obtained from the induced-orientation theory for a $J = 1 \rightarrow 2$ transition in one dimension is given by

$$f = -\alpha(v - v_B) = -\alpha v - \kappa z, \tag{44}$$

where

$$\kappa = \frac{g_{J1}\mu_B}{\hbar k}\frac{dB}{dz}\alpha, \tag{45}$$

$$\alpha = \frac{120}{17}\frac{-\delta\Gamma}{5\Gamma^2 + 4\delta^2}\hbar k^2 \tag{46}$$

(Ref. 26), so that

$$\kappa = g_{J_1}\mu_B k\frac{dB}{dz}\frac{120}{17}\frac{\delta\Gamma}{5\Gamma^2 + 4\delta^2}. \tag{47}$$

The spring constant is increased above its Doppler-theory value, and the variation with detuning and intensity is changed. The friction is similarly increased, as is now familiar from the study of optical molasses.

Molmer[5] has reported calculations of the friction parameter in a three-dimensional σ^+-σ^- molasses for the case in which the polarization of the three-dimensional standing-wave field is everywhere linear. For a fixed value of intensity per trapping beam, he obtains a result 0.59 times that given by the one-dimensional calculation. Therefore, for a $J = 1 \rightarrow 2$ transition, the spring constant in three dimensions may be smaller than that given by Eq. (47) by the same factor. A further calculation to confirm this would be useful, as would calculations for other transition schemes.[34]

A three-dimensional version of the trap is realized by means of a spherical quadrupole magnetic field with three pairs of laser beams, one pair propagating along each coordinate axis (other geometries are also possible). With the correct choice of polarizations it is evident that trapping is obtained along each of the coordinate axes, but further consideration is required for one to deduce that trapping is obtained for all directions in space. The original work of Raab *et al.*[1] used a numerical calculation to confirm that trapping is indeed obtained in all directions. It is useful to have an intuitive way of understanding this, which is obtained as follows. Consider a laser beam propagating along a direction z_b with σ^+ polarization, defined for a quantization axis along z_b. The polarization vector is

$$\epsilon = -\frac{1}{\sqrt{2}}(\hat{x}_b + i\hat{y}_b). \tag{48}$$

If the direction z_b makes an angle θ with the z axis, then $\hat{x}_b = \hat{x}\cos\theta - \hat{z}\sin\theta$, $\hat{y}_b = \hat{y}$, so that

$$\Rightarrow \epsilon = -\frac{1}{\sqrt{2}}(\hat{x}\cos\theta + i\hat{y} - \hat{z}\sin\theta). \tag{49}$$

In terms of the three spherical tensor components for a quantization axis along z, this polarization vector is

$$\epsilon = \frac{1}{2}(\cos\theta + 1)\epsilon_+ - \frac{1}{2}(\cos\theta - 1)\epsilon_- + \frac{1}{\sqrt{2}}(\sin\theta)\epsilon_0, \tag{50}$$

using $\epsilon_+ = -(1/\sqrt{2})(\hat{x} + i\hat{y})$, $\epsilon_- = (1/\sqrt{2})(\hat{x} - i\hat{y})$, $\epsilon_0 = \hat{z}$.

Thus the σ^+ beam along z_b causes ΔM_J of $+1$, -1, and 0 transitions in the proportions $(1/4)(\cos\theta + 1)^2$, $(1/4)(\cos\theta - 1)^2$, and $(1/2)\sin^2\theta$, respectively. Now let the quantization axis always be along the direction of the magnetic field in the trap. If one inspects a map showing the direction of the field (Fig. 3), one can quickly convince oneself, using Eq. (50), that the force on a stationary atom resulting from each pair of laser beams is always such as to reduce the radial coordinate of the atom. For example, when the field lines are vertical, the horizontal beams give no net restoring force; when the field lines are at 45° to the axes, each laser beam contains predominantly the correct polarization for trapping rather than antitrapping; the proportions of σ^+, σ^-, and π are 0.73, 0.02, and 0.25, respectively.

A further result of Raab's calculation (Fig. II.11 of Ref. 14) is that the force for points on the (1, 1, 1) diagonal

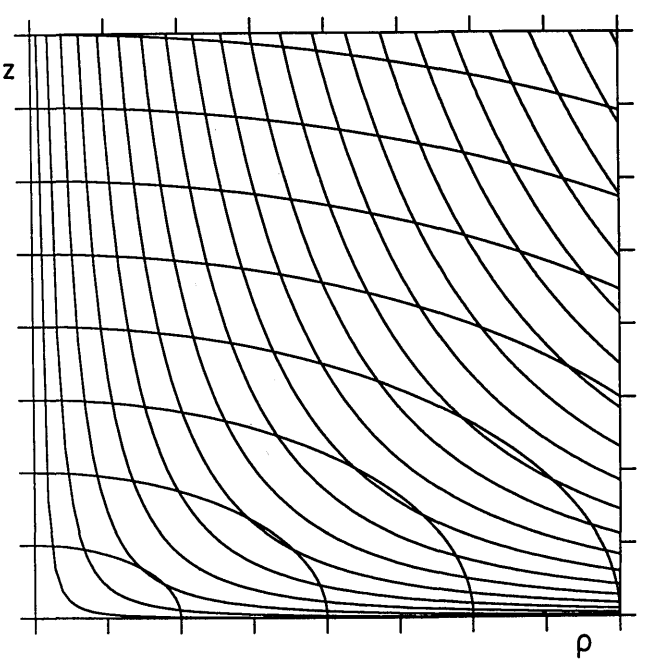

Fig. 3. Magnetic-field lines and contours near the center of the trap. The field lines satisfy $dz/d\rho = B_z/B_\rho = -2z/\rho$. The contours of constant field are ellipses.

is directed not toward the origin but at an angle of ~9° to the (1,1,1) diagonal, with the z component larger than the other components. This force is also smaller in magnitude, that is, its magnitude (for a stationary atom) is ~60% of that of the force along the z axis for the same value of the magnetic field. Much of this reduction is explained by Eq. (50) and so can be expected for the polarization-gradient forces also. The effect on the cloud shape will be to make the cloud fatter along the diagonal directions than would be the case for an ellipsoid. In other words, the cloud becomes more rectangular.

The magnetic field in the trap may be calculated by numerical integration or by using the formulas given in Ref. 35. For points near the origin the field resulting from a pair of coils with opposing currents is given by

$$B_z = b_1 z + b_3\left(z^3 - \frac{3}{2}z\rho^2\right) + \ldots, \tag{51}$$

$$B_\rho = -\frac{1}{2}b_1\rho + b_3\left(-\frac{3}{2}\rho z^2 + \frac{3}{8}\rho^2 z\right) + \ldots, \tag{52}$$

where

$$b_1 = \frac{\mu_0}{4\pi}\frac{12NI\pi R^2 A}{(R^2 + A^2)^{3/2}}\frac{1}{(R^2 + A^2)}, \tag{53}$$

$$\frac{b_3}{b_1} = \left(\frac{5}{6}\right)\frac{4A^2 - 3R^2}{(R^2 + A^2)^2}. \tag{54}$$

Here R is the radius of the coils, $2A$ is their separation, and NI is the number of current turns. For A and R of similar sizes the field given by including terms of up to third order is accurate to within 5% for distances from the origin up to 0.6 times the coil radius. When one is considering the motion of atoms held in the trap, the first-order terms usually give sufficient accuracy on their own. If all dimensions are scaled uniformly, the fields will vary as $1/R$, derivatives as $1/R^2$, etc.

D. Friction Parameter

Molmer has calculated the friction parameter for a three-dimensional σ^+-σ^- molasses, with a $J = 1 \rightarrow 2$ transition.[5] His numerical result can be fitted (within 10%) by the formula

$$\alpha_{\text{io}} \simeq 4.2\frac{\delta\Gamma}{5\Gamma^2 + 4\delta^2}\hbar k^2 \tag{55}$$

for $kv \ll \Gamma\delta$, $\Omega \ll \Gamma$. The structure of this formula is based on Dalibard and Cohen-Tannoudji's one-dimensional analytical result,[26] which we used in Eq. (47). At $\delta = \Gamma$ one obtains $\alpha/4m = 3$ kHz. From Eq. (45) the field gradient necessary to yield critical damping [relation (33)] is 100 G/cm ($g_F = 0.25$ for the $F = 4$ ground state of cesium and $m = 2.2 \times 10^{-27}$ kg). In practice gradients from 5 to 20 G/cm are usually used, so that the motion is almost always overdamped, in contrast to the result of Doppler theory.

So far both the friction parameter and the spring constant have been obtained in the case for which the polarization of the radiation field is everywhere linear but varying in magnitude and direction. However, Fig. 2 indicates that for a different choice of the relative phase between the standing waves one obtains alternating circular polarization states and hence Sisyphus cooling. An approximate value for the friction parameter in this case may be obtained from Molmer's calculation for three-dimensional lin ⊥ lin molasses for a $J = 1 \rightarrow 2$ transition. His numerical calculation (Fig. 7b of Ref. 5) is reproduced by the formula

$$\alpha_{\text{sis}} \simeq \hbar k^2\frac{3\delta}{20\Gamma}\left(\frac{3\delta^2 + 14\Gamma^2}{\delta^2 + \Gamma^2}\right). \tag{56}$$

(This is ~6 times smaller than the one-dimensional Sisyphus result.[5,26]) For detunings above a few linewidths, α_{sis} is an order of magnitude larger than α_{io}. Thus one can expect to see dramatic variations in the size of the friction parameter as the relative phase of the standing waves in the trap is varied. This would reveal itself as a variation in the size of α/κ, the time scale of damped motion to the trap center [Eq. (30) and relation (34)]. One might also expect κ to be reduced when α increases, since the pattern of polarization is not ideal for induced orientation when the Sisyphus effect is present. We reported measurements of this damped motion in our earlier paper,[3] where we pointed out that the results implied a value for the friction parameter that is much larger than could be explained by Doppler theory. We now add a further remark, namely, that our results were not consistent with Eq. (45) either; but they are consistent if the friction coefficient is given by α_{sis}.

E. Cloud Radius

At low density the radius of the trapped cloud is given by Eq. (18). The temperature in optical molasses is roughly independent of the predominant type of polarization gradient, leading to a cloud radius given by

$$\langle r_z^2\rangle \simeq 0.17\frac{\hbar\Gamma}{g_J\mu_B(\mathrm{d}B/\mathrm{d}z)k}\left(\frac{\Omega}{\Gamma}\right)^2\left(\frac{5\Gamma^2 + 4\delta^2}{\Gamma^2 + 4\delta^2}\right). \tag{57}$$

The spring constant here is reduced from the value in Eq. (47) by a factor of 0.59 to suit a three-dimensional trap, and the temperature is taken from the lin ⊥ lin theory in Ref. 5 (1.8 times higher than that for the one-dimensional result). The value of Ω is taken to be the Rabi frequency for any one of the laser beams. For cesium at $\Omega = \Gamma/2$, with a field gradient of 10 G/cm, one obtains a radius of 9 μm. The radius at which the Larmor frequency becomes equal to the optical pumping rate [inequality (37)] or to the light shift, on the other hand, is ~300 μm for this case. Thus the trap confines the cloud well inside the low-field region (see also Section 9 below), and we are justified in ignoring high-field effects once the atoms have settled in the trap. Relation (57) gives a radius that is roughly independent of laser detuning and increases with intensity (Fig. 4), a result in marked contrast to that of the Doppler theory, which gives

$$\langle r_z^2\rangle \simeq \frac{\hbar\Gamma}{g\mu_B(\mathrm{d}B/\mathrm{d}z)k}\frac{1}{\Omega^2}\frac{(\delta^2 + \Gamma^2/4)^3}{2\delta^2\Gamma^2}. \tag{58}$$

The radius we observe in our trap for cesium is a few times larger than that indicated by relation (57). This implies that relation (57) either underestimates the temperature or overestimates the spring constant when the transition is $4 \rightarrow 5$ instead of $1 \rightarrow 2$. Our measurements

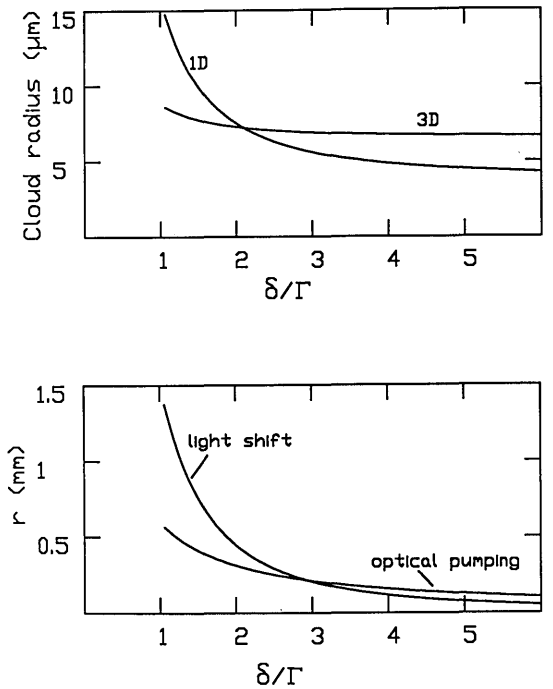

Fig. 4. Various significant radii in the trap. Top, the radius of the cloud, as given by relation (57) (3D) and by a calculation in which all the parameters are taken from the one-dimensional induced-orientation theory (1D). Bottom, radii at which the Larmor frequency is equal to the optical pumping rate and to the light shift. Note the different vertical scales. The example given is for $\Omega = \Gamma/2$ and a field gradient of 10 G/cm.

of these parameters imply that it is the temperature that is increased, though there is further analysis to do, since the temperature itself is influenced by the density and magnetic-field gradient when these are high. A further comment is that it is easy, in practice, to exceed the density at which photon pressure in the cloud is significant, so that one obtains the low-density radius [relation (57)] only by deliberately loading small numbers of atoms or by operating at a low laser intensity.

5. CLOUD DENSITY, COLLECTIVE EFFECTS

We now estimate the density of atoms that can be achieved in a magneto-optical trap. This is interesting from the point of view of observing cold collisions and collective effects such as Bose–Einstein condensation. Also, any nonlinear-optical properties of the trapped cloud are likely to be easier to detect at high densities. As more and more atoms are added to the trap, the first effect that limits the density of the trapped cloud is photon scattering within it, as is discussed in Section 3. The number density of atoms for which the repulsive and attractive parts of the force are equal is given by Eq. (25). Using our estimate for the (three-dimensional) spring constant, we have

$$n \simeq 12\left[\frac{g\mu_B(\mathrm{d}B/\mathrm{d}z)I_S}{\hbar^2 kc\Gamma^2}\right]\frac{(\Omega^2/2+\delta^2+\Gamma^2/4)^3 2(2\Omega^2+\Gamma^2)}{(5\Gamma^2+4\delta^2)\delta\Gamma(\Omega^2/2)^2}, \tag{59}$$

where Eq. (21) and relation (29) were also used. This relation is valid only for the range of intensities and detunings for which the induced-orientation formula for the spring constant is accurate. In other words, n will not in fact tend to infinity as the intensity tends to zero, and the equation overestimates n when $\Omega^2/\delta\Gamma$ is greater than ~0.5, since the polarization-gradient theory was calculated for the regime of low intensity. The limiting density goes up with the field gradient, since this increases the spring constant without affecting the photon scattering in the cloud. The limiting density is also increased at low intensities and high detunings, since the spring constant is independent of intensity and falls off with detuning more slowly than the photon-scattering repulsive force. Relation (59) can be regarded only as an order-of-magnitude estimate, but it reproduces the experimentally observed limit of approximately 5×10^{10} atoms/cm^3 (Ref. 18) at typical values for the parameters (i.e., $\mathrm{d}B/\mathrm{d}z = 10$ G/cm, $\Omega = \delta = 2\Gamma$). It is interesting to note that a limiting density of 1 atom/λ^3 (where λ is the wavelength) is fairly easy to obtain. At a field gradient of 20 G/cm one obtains

$$12\frac{g\mu_B(\mathrm{d}B/\mathrm{d}z)I_S}{\hbar^2 kc\Gamma^2} = 4.6 \times 10^9 \text{ atoms/cm}^3 = \frac{1}{(7.1\lambda)^3}.$$

A limiting density of 1 atom/λ^3 is then produced at, for example, $\Omega = \Gamma/2$ and $\delta = 2\Gamma$. At this density the resonant dipole–dipole interaction shifts the excited-state energy level by one linewidth of the transition [Eq. (9)], so that the theory we have been using begins to break down. This is not significant for our highly approximate discussion, but it shows that a more accurate treatment of the collective motion may have to allow for the influence of the molecular potential on the radiation force. An experimental measurement of the limiting density, as a function of laser detuning, would produce useful information for understanding this situation. The results are significant to the two-dimensional compression of atomic beams also.[7]

With a cloud radius of ~50 μm, the number of atoms in a cloud with 1 atom/λ^3 is $\sim 8 \times 10^5$. To estimate how easy this density is to obtain, one needs to estimate the loss from the trap. The results in Ref. 8 indicate that the loss will be dominated by hyperfine-changing collisions between ground-state atoms in the trap. Using $\beta = 10^{-11}$ cm^3/s, one obtains a trap lifetime $1/\beta n = 0.06$ s. [β is the collisional loss parameter defined by Eq. (5); the value is taken from Ref. 8.] To obtain the required number of trapped atoms in a steady state, therefore, one must load 1.3×10^7 atoms/s. This rate is of the order of magnitude of the capture rate for a trap of radius 4 mm in an atomic vapor cell (Subsection 2.A) when the laser intensity is near the saturation intensity.

A possible experimental method for obtaining high steady-state trapped densities in a simple vapor-cell apparatus would be to optimize the loading rate in the outer region of the trap while optimizing the conditions for high density at the center of the trap. For example, one could use large-radius trapping beams, whose intensity profiles have a minimum rather than a maximum at the center.

6. EXPERIMENTAL ARRANGEMENT

Although the magneto-optical trap has been used in a variety of experiments as a source of cold atoms or as an

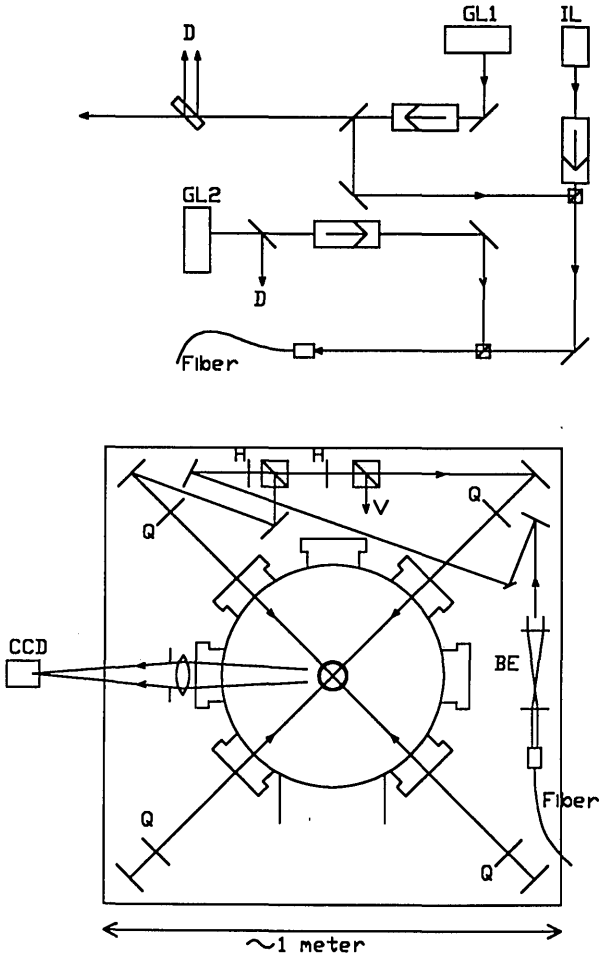

Fig. 5. Trapping experiments. Top: GL1, GL2, grating-stabilized lasers tuned to $F = 4 \rightarrow 5$ and $F = 3 \rightarrow 4$ transitions, respectively; IL, injection-locked laser; D, frequency diagnostics (saturated absorption cell); arrowed boxes, optical isolators. Bottom: BE, beam expander; H's, half-wave plates; Q's, quarter-wave plates; V, vertical beams; CCD, video camera. The diagram is not exactly to scale, but rough dimensions are indicated.

interesting many-body system, the task of measuring its basic properties, such as the size of the confining force, still has not been carried out with any great precision. The equations for the force, given above, are valid in the regime of low saturation of the atomic transition for atoms moving with low velocity near the center of the trap, i.e., satisfying the conditions

$$\hbar k v, \mu_B B < \Omega^2/6\delta \ll \hbar\Gamma, \tag{60}$$

where Ω is the Rabi frequency per laser beam. We have shown that these conditions are satisfied once the atoms have settled in the trap. Here we describe measurements that test the predictions for the spring constant. Before these measurements are presented (in Sections 8 and 9) we describe our experimental apparatus and give a measurement of the cross section for collisional loss from the trap (Section 7).

The arrangement used for the trapping experiments is shown in Fig. 5. Our apparatus has not been described elsewhere, so we give most of the details here. The trapping light was provided by an injection-locked 50-mW laser diode (STC), from which 12 mW was coupled into a single-mode fiber. The injecting laser was a diode stabilized by feedback from a diffraction grating positioned a few centimeters away.[36] Faraday-effect optical isolators (each providing 33-dB isolation) were used to shield the injecting laser from the injected one and to prevent optical feedback from the fiber end. A second grating-stabilized diode laser provided repumping light, typically 1 mW of power coupled into the fiber. This light was tuned to the $F = 3 \rightarrow 4$ transition in cesium to pump atoms optically out of the lower hyperfine level of the ground state. A beam splitter reflected 70% of the light out of each grating–diode cavity. This ratio implies a feedback fraction into the diode of a few percent, which was sufficient to yield strong feedback. (In our ongoing research we now use the same arrangement without the beam splitter, using the zeroth order from the grating as the laser output. This gives less output power, but the increased feedback makes the system more reliable.) Each laser cavity was mounted upon a small temperature-stabilized Invar bar, giving a long-term drift of ~20 MHz/h before active stabilization. The lasers were set to the correct frequencies by saturated absorption spectroscopy in two cesium-vapor cells. For the main laser a computer-controlled servo system was used. The computer first scanned the laser slowly over the saturated absorption profile (a digital-to-analog converter supplied a few volts to a piezo device on the grating) while monitoring the transmission of a weak beam through the vapor cell. The program then used this information to set the grating to the correct position for any given detuning and continued to monitor the weak-beam transmission to provide a servo loop to compensate for drifts of the laser cavity. This system enabled us to switch the laser, in a few milliseconds, to any required frequency with an accuracy of 0.5 MHz. The repumping laser frequency was set manually.

The single-mode fiber was used primarily to improve the spatial quality of the beams; improved quality was necessary for reproducible measurements of the trap parameters. An objective permanently fixed to the fiber end produced a beam with a small radius, which was then expanded to a $1/e^2$ radius of 3.3 ± 0.1 mm. The beam expander used lenses of focal lengths 5 and 15 cm, producing a Gaussian beam with intensity ripples at the 10% level. When lenses of shorter focal lengths were used, we found that the spatial quality was significantly reduced.

The beam from the fiber was divided by polarizing cube beam splitters, with half-wave plates that could be rotated to set the division ratio. We found that if simple dielectric beam splitters were used then the beam quality was reduced because of interference fringes originating from multiple reflections in the beam splitters. The half-wave-plate–polarizing-cube arrangement also has the advantage that the degree of polarization of the light is maintained, and the division ratio can be adjusted easily. The horizontal standing waves were formed by retroreflection, but the vertical wave (not shown in Fig. 5) was not. Instead the beam was once again divided by a half-wave plate and a polarizing cube beam splitter, and the two resulting beams formed the upward- and downward-pointing trapping light. This enabled us to introduce a controlled intensity imbalance in this beam pair.

The optical fiber was a polarization-preserving fiber, and the light beams from the main and the repumping

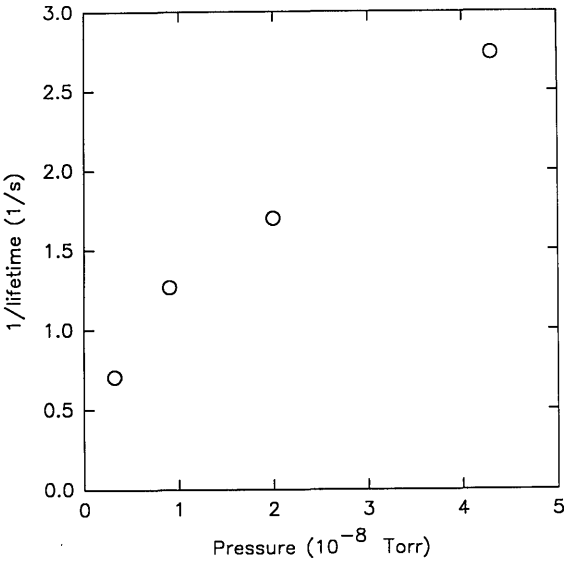

Fig. 6. Inverse of the trap lifetime as a function of background pressure. The trapping light was at 6-MHz detuning, 7 mW/cm^2 per beam. The experimental uncertainty in the lifetime measurements is indicated by the size of the symbols. The pressure given is that indicated by the ion gauge (calibrated for N_2). If the background gas is cesium, the actual pressure is less than that indicated by the gauge.

lasers were sent into it with orthogonal linear polarizations. With this method, when the three pairs of trapping beams were formed with equal-intensity radiation at the $F = 4 \rightarrow 5$ frequency, most (75%) of the repumping ($F = 3 \rightarrow 4$) light was in the first horizontal beam pair. It was useful to have most of the repumping light in the horizontal beams rather than in the vertical ones, since then the predictions for the vertical displacement of the trapped cloud were less influenced by the radiation force associated with the repumping light.

The atoms were loaded into the trap from a background vapor of cesium in the vacuum can at pressures of less than 10^{-9} Torr. The vacuum system was a large stainless-steel apparatus pumped by a single oil diffusion pump with a liquid-nitrogen-cooled baffle. The experiments described here could be done in a simpler system based on a glass vapor cell evacuated by an ion pump.

Not shown in Fig. 5 are three pairs of field nulling coils. These formed a rectangular frame around the vacuum can, with dimensions 1 m × 1 m × 0.7 m. The up–down coil pair was used in the imbalance measurements described in Section 9 to provide the offsetting vertical magnetic field.

Light from the trap was gathered by a single symmetric convex lens of focal length 15 cm apertured at diameter 4 cm. This lens formed an image (at unit magnification) with a resolution limited by spherical aberration to ~10 μm, which equaled the pixel size in the camera. Increasing the aperture at the lens merely degraded the image; an improved optical system would be required for increased image brightness.

7. CROSS SECTION FOR COLLISIONAL LOSS

The lifetime for atoms to remain in the trap was measured by replacing the CCD camera in Fig. 5 by a photomultiplier tube and recording the decay of fluorescence from the trap after the loading was blocked. (For these measurements the trap was loaded from an atomic beam rather than from a vapor.) The decay was exponential. The variation of the inverse of the lifetime with background pressure is shown in Fig. 6. If the pressure alone were varied, one would expect this graph to show a straight line through the origin, with slope $\sigma/(\pi m k_B T/8)^{1/2}$ [Eq. (11)]. However, for these measurements we aimed only to obtain a rough estimate of the effect of background pressure, and the pressure change was obtained by degassing (for a few seconds) one of two ion gauges in the vacuum system. The problem with this method is that the molecular composition of the background gas probably changed along with the pressure. If we assume that at low pressures the background gas was predominantly cesium, whereas at higher pressures it had some other composition, then the shape of the curve in Fig. 6 indicates that the cross section for cesium–cesium collisions (causing loss from the trap) is higher than that for collisions with other species. This is what was predicted in the discussion in Subsection 2.B, where the large cross section was associated with the resonant dipole—dipole interaction. The measurements at pressures below 10^{-8} Torr indicate a cross section $\sigma = 60^{+40}_{-20} \times 10^{-14}$ cm^2 for collisions with cesium, where the error is associated with the uncertainty in the calibration of the pressure gauge. (In calculating σ we assume that the gauge is ~2.7 times as sensitive for cesium gas relative to N_2; this rough estimate is based on the figures in Ref. 37.) This result is consistent with the discussion in Subsection 2.B, though somewhat larger than the value quoted in Ref. 9. The difference with Ref. 9 may be due to the different parameters of the trap (e.g., beam radius and intensity). A more systematic study of the trap lifetime would be useful. One could measure the background pressure of cesium directly by detecting absorption of a probe laser beam sent through the vacuum chamber.

8. INTERFERENCE FRINGES

Our aim in performing the imbalance measurements described in Section 9 was to obtain sufficient accuracy to give a quantitative comparison with the theory. To this end, we first studied in more detail the effect of interference fringes in the trapping light. The fringes were observed by using a low field gradient (2.5 G/cm in the vertical direction) in order to obtain a large cloud. At a low field gradient it is important to ensure that each pair of beams is accurately counterpropagating; otherwise too few atoms will be loaded into the trap. This is because the misaligned beams produce unbalanced radiation forces in the region where the beams do not overlap; these forces push incoming atoms away from the trap. Once all the beams are aligned, one or more of the beams may be misaligned and the fringes observed.

We found that only a single one of the six beams need be misaligned for the fringes to appear. Measurements of the video image of the fringes, for various angles of misalignment of a single beam, gave a value of $(1.09 \pm 0.05)\lambda/\theta$ for the fringe separation, where θ is the angle (in radians) between the misaligned beam and its partner and λ is the wavelength of the light (852 nm). This result is consis-

tent with the fringe separation implied by Fig. 2. Misaligning a second beam, propagating at right angles to the first, did not affect the fringe separation until the angle of misalignment of the second beam became comparable with that of the first—the inverse of the separation was not simply proportional to the difference in angles $\theta_1 - \theta_2$.

Under the conditions of our experiment, when the trapping beams were well aligned they would typically have residual misalignments of ~0.3 mrad, leading to fringe separations of ~3 mm. In this regime other properties of the radiation field are noticeable, such as the changing direction of the Poynting vector, producing circular motion of the atoms,[31] and wave-front irregularities, leading to millimeter-scale interference effects. Such irregularities in the radiation field are unavoidable (unless significant extra care is taken with the quality and the stability of the optics). To assess the influence of such irregularities on the imbalance measurements described in Section 9, we set up a system of fringes with separations of 0.3 mm and observed the trapped cloud in a vertical field gradient of 15 G/cm, which gave a vertical cloud diameter of 0.3 mm. The intensity of the fluorescence was observed to vary slightly as the fringes moved, but the time-averaged position of the center of the cloud was not changed by a detectable amount. (By time averaged we mean the position as estimated visually by observing a vertical profile of the trap fluorescence on an oscilloscope.) We infer that the position measurements used to deduce the spring constant of the trap were not significantly affected by the presence of interference fringes larger than the trapped cloud.

9. INTENSITY IMBALANCE MEASUREMENTS

Our first measurements of the spring constant of the trap[3] had a statistical uncertainty of approximately a factor of 1.5 and a systematic uncertainty of similar magnitude. The systematic error was related to the uncertainty in the calculation of the force exerted by a pushing beam incident upon the trap. A method in which the theoretical uncertainties are under greater control is to use only the six beams forming the trap and to investigate the effect of intensity imbalances. The theoretical expectations for this type of experiment are as follows.

With all the trapping beams having exact circular polarization and balanced intensities, the trapping force always confines the atoms to the zero of the magnetic field. In other words, if an additional stray field is added to the quadrupole field from the trapping coils, the cloud simply moves so that its center is always at the field zero. Now consider a pair of beams having different intensities I_1 and I_2. Let w be a parameter defining the degree of imbalance, thus:

$$w = \frac{I_1 - I_2}{I_1 + I_2} \tag{61}$$

$$\Rightarrow I_1 = (1 + w)\frac{I_1 + I_2}{2}, \tag{62}$$

$$I_2 = (1 - w)\frac{I_1 + I_2}{2}. \tag{63}$$

For the induced-orientation theory, the effect of an intensity imbalance is calculated by adapting Eq. (5.9) from the paper of Dalibard and Cohen-Tannoudji.[26] Substituting $s_+ = s_0(1 + w)$, $s_- = s_0(1 - w)$ [cf. Eq. (63)], one obtains

$$f = \frac{120}{17}\hbar k\frac{\delta\Gamma k v}{5\Gamma^2 + 4\delta^2} + \frac{10}{17}\Gamma s_0 w\hbar k. \tag{64}$$

This is valid in the low-velocity domain, when the solution need be considered only to first order in velocity and when the imbalance itself is small, so that one can use the original calculations of the ground-state populations and coherences. Replacing kv by $g_J\mu_B B/\hbar$, one deduces that the trapped cloud is centered at

$$B = \frac{\hbar}{g_J\mu_B}\left(\frac{5\Gamma^2 + 4\delta^2}{\Gamma^2 + 4\delta^2}\right)\frac{\Omega^2}{6\delta}w. \tag{65}$$

At large detunings the displacement is proportional to the light shift. The range of fields (or velocities) for which the induced orientation enhances the radiation force is also proportional to the light shift, being equal to roughly $\Omega^2/6\delta$ (see Refs. 26 and 34). Therefore the intensity imbalance that shifts the trapped cloud to the edge of the region in which the spring constant is enhanced is given by

$$w \simeq \frac{\Gamma^2 + 4\delta^2}{5\Gamma^2 + 4\delta^2} \tag{66}$$

$$\simeq 1 \qquad \text{at large detunings.} \tag{67}$$

The imbalance w equals 1 when one beam of the pair has zero intensity. The approximation used to derive Eq. (65) break down before this point, but it is clear that for any reasonably small imbalance the trapped cloud is well within the region for which the polarization gradient theory applies. For example, with an imbalance $w = 0.05$, at $\Omega = \Gamma/2$ and $\delta = \Gamma$, the field at the center of the cloud is 0.03 G. We have observed the cloud changing shape as it reaches the high-field region when the imbalance is near $w = 0.5$ (see Subsection 9.D).

There is a sharp contrast between Eq. (65) and the Doppler theory, for which at low intensities the total force for a $0 \rightarrow 1$ transition is

$$f = \hbar k\gamma(s_1 - s_2) \tag{68}$$

$$= -\alpha v - \kappa z + \hbar k\Gamma w s_0, \tag{69}$$

giving a cloud centered at

$$B = \frac{\hbar\Gamma}{g\mu_B}\left(\frac{\delta^2 + \Gamma^2/4}{2\delta\Gamma}\right)w. \tag{70}$$

This provides a comparison between the Doppler and the sub-Doppler regimes that is easy to test experimentally. Also, if the cloud extends beyond the edge of the low-field (sub-Doppler) region, Eq. (70) indicates that the outer part of the cloud will be particularly sensitive to intensity imbalances for typical values of intensity and detuning.

A. Experimental Method and Accuracy

Equation (65) indicates that the position of the trap center for a given imbalance is dependent mainly on the ratio of the intensity to the detuning of the trapping light. Thus, to obtain good experimental accuracy, one requires accurate knowledge of the size of the intensity imbalance, the position of the cloud, the absolute intensity of the light,

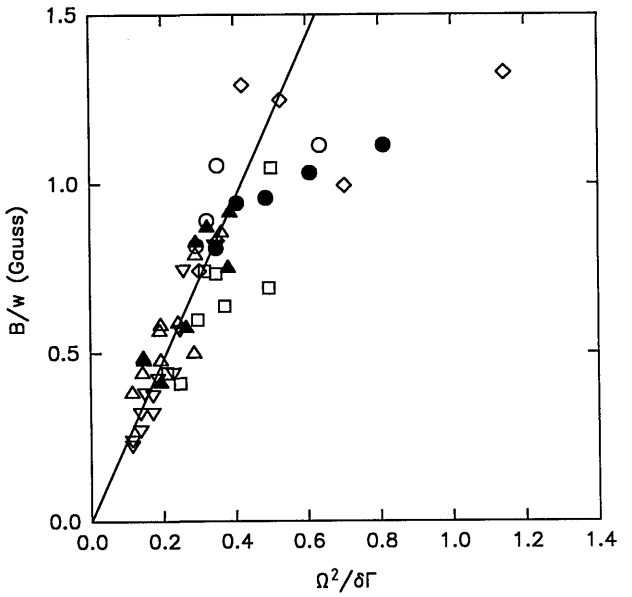

Fig. 7. Imbalance measurements. All the data are shown. The vertical axis shows the magnetic field, in gauss, to which the trapped cloud moves, per unit intensity imbalance w in the vertical beams. The straight line is a fit to the data points for which $\Omega^2/\delta\Gamma < 0.4$. The symbols indicate the intensity per beam as follows: $I/I_S = 2.3$, ●; 2, ◇; 1.7, ○; 1.4, □; 1, ▲; 0.7, ▽; 0.55, △.

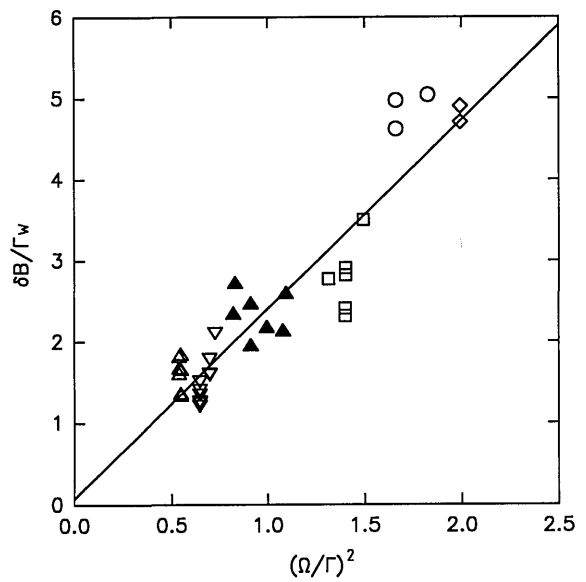

Fig. 8. Imbalance measurements as in Fig. 7, rescaled by the expected detuning dependence in order to reveal the dependence on the average intensity per trapping beam. Only the data points for detunings larger than 10 MHz and $\Omega^2/\delta\Gamma$ smaller than 0.4 are included. The line is a linear fit to the data.

and the detuning. We obtained accurate and reproducible intensity imbalances in the vertical beam pair by mounting a half-wave plate in a micrometer-driven rotating mount in front of the polarizing beam splitter that provided the two vertical beams. If the transmissions of the beams from the splitter to the trap are t_1 and t_2, then the imbalance is given by

$$w = \frac{I_1 - I_2}{I_1 + I_2} = \frac{t_1 \cos^2(2\theta) - t_2 \sin^2(2\theta)}{t_1 \cos^2(2\theta) + t_2 \sin^2(2\theta)}, \quad (71)$$

where θ is the angle of the half-wave plate. As long as t_1/t_2 is not significantly different from 1, any changes in the values of t_1 and t_2 (for example, owing to beam movements) simply result in a small shift in the value of θ that gives $w = 0$. Errors associated with this zero shift were avoided by taking a series of measurements at different values of θ for each chosen laser intensity and detuning. A straight line was fitted through each set of values of imbalance versus trap position, and the slope of this line provided one data point in the results shown in Figs. 7–10.

The accuracy in measurements of the cloud position was improved by adopting the following technique. For a given intensity imbalance set by the half-wave plate, instead of our trying to estimate how far the cloud had moved across the trapping beams, a vertical field was imposed (using the up–down field-nulling coils) so that the

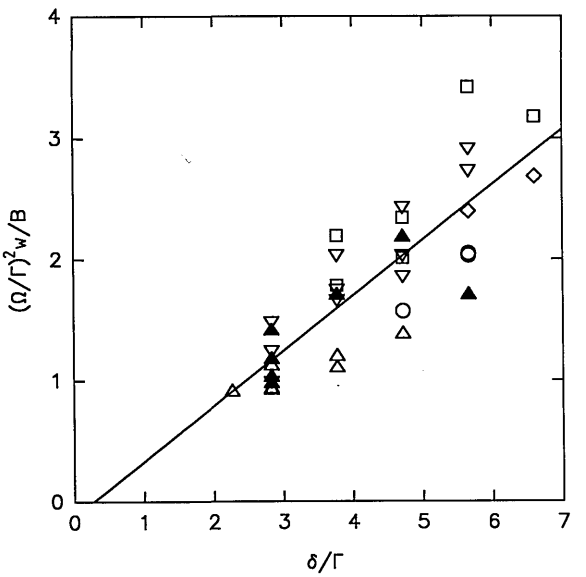

Fig. 9. Imbalance measurements. The data are as for Fig. 8, rescaled in order to reveal the dependence on detuning. The line is a linear fit.

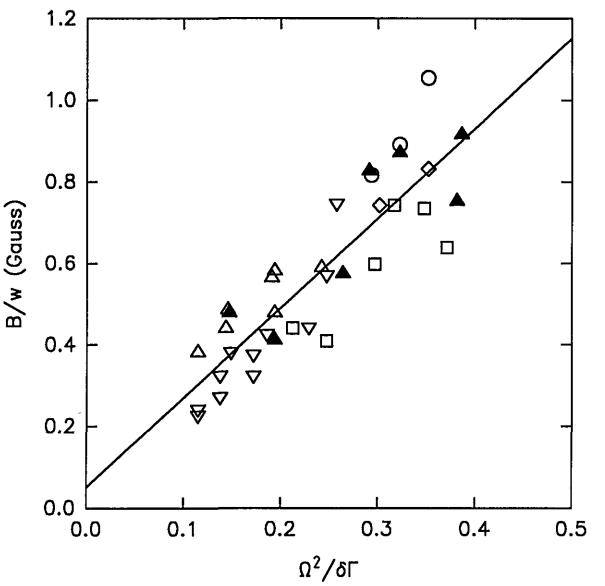

Fig. 10. Imbalance measurements, showing the data at small values of the light shift and detunings larger than 10 MHz.

cloud moved back to the same position for each measurement, and the value of this vertical field (i.e., of the current in the up–down coils) was recorded. The accuracy could be made equivalent to approximately one fifth of the diameter of the cloud by observing a vertical profile of the cloud on an oscilloscope that monitored the CCD video signal and returning the cloud center to a fixed point at the center of the oscilloscope screen. This method had the important advantage of always recording the data with the cloud at the same point in the radiation field, so that the light intensity at the cloud did not vary for each set of position-versus-imbalance measurements.

The final uncertainty in our measurements was limited by the uncertainty in the detuning and the intensity of the light. The detuning was reliable only to ~0.5 MHz, and the intensity at the trapped cloud would vary with changes in the beam profile and with the total power in the beam. The power in the vertical beam pair was affected by movements of the optical fiber. We kept track of such changes by checking the power in the vertical beams periodically as the experiments were performed. In the analysis of our results presented below we used measurements only at detunings greater than 15 MHz, so that the error associated with each detuning value was less than 4%. The statistical spread in our data points indicated uncertainties at roughly the 10% level, probably resulting mainly from the uncertainty in the intensity. With ~40 data points, our final results have statistical uncertainties of ~3%, giving a fairly accurate test of the theory of the trap. However, there is the possibility of a 20% systematic error in the intensity values, which limits the absolute accuracy of our final result. An error in the value used for the vertical magnetic field, obtained from the current in the up–down nulling coils, would also be a systematic error in our results. We estimate that this error is less than 3%.

A further experimental technique enabled us to obtain data points for large detunings when the loading into the trap was not efficient. We would load the trap at the optimum detuning of ~6 MHz and then switch the detuning to the required setting (e.g., 25 MHz) in less than 1 ms. The trapped cloud would simultaneously move to a new position and decay, since the loading no longer balanced the loss. The motion of the cloud center was sufficiently fast and the loss sufficiently slow that the new equilibrium position of the cloud could be observed before the cloud's image completely disappeared. Typically the process would be repeated several times (over a period of 10 s or so) to enable the experimenter to gain a good indication of the position of the disappearing cloud.

B. Results

We present in Figs. 7–10 a summary of the results. A single set of 52 points is compared with the expectations based on Eq. (65). We rewrite Eq. (65) in the form

$$\frac{B}{w} = \frac{\hbar\Gamma}{6g_F\mu_B} d \frac{\Omega^2}{\delta\Gamma}, \tag{72}$$

where

$$d = \left(\frac{5\Gamma^2 + 4\delta^2}{\Gamma^2 + 4\delta^2}\right). \tag{73}$$

B/w is the value of the field at the cloud position per unit intensity imbalance, i.e., the measured quantity. The parameter d is a function of δ/Γ; its value varies between 1.12 and 1.03 for detunings between 15 and 30 MHz, so that it is a relatively small adjustment. Indeed, for transitions $F \rightarrow F + 1$ with $F > 1$ the dependence of the radiation force on detuning changes slightly: The $5\Gamma^2$ in the numerator of Eq. (73) becomes $\sim 1\Gamma^2$, so that d is almost exactly equal to 1.[34] We present our data in a form that tests for $B/w \propto \Omega^2/\delta\Gamma$, i.e., we take $d = 1$. Equation (72) is based on a one-dimensional rather than a three-dimensional theory. We assume that the one-dimensional theory gives the correct functional form of the force in a three-dimensional case, and our experimental results will give the magnitude of the force.

Figure 7 shows the measured values of B/w as a function of $\Omega^2/\delta\Gamma$. We see that the data fall below the straight line when the light shift is large; in this region the theory is no longer accurate (B/w versus $\Omega^2/\delta\Gamma$ is calculated in the case of low intensities and large detunings). It is interesting to compare Fig. 7 with Fig. 2b of Ref. 38; the dependence on $\Omega^2/\delta\Gamma$ of the temperature in molasses is similar to that of the field per imbalance in the trap, though the two cases result from different features of the radiation force.

Figures 8–10 show only the data for which $\Omega^2/\delta\Gamma$ is less than 0.4, so that one expects the points to fall on a straight line. To test the dependence on intensity and detuning, Figs. 8 and 9 show the values of B/w rescaled by the expected detuning and intensity factors, so that the dependence on the other parameter is revealed. The results are all consistent with the theory. A linear fit with two parameters (the gradient and the intercept of the line) in each case produces a line passing through the origin, within the experimental accuracy. Figure 10 shows the dependence on $\Omega^2/\delta\Gamma$ for small light shifts.

C. Discussion

If, in each case, one forces the fitted line to pass through the origin, one obtains a gradient of (2.39 ± 0.07) G. [For a linear fit not constrained to pass through the origin, the gradient is (2.24 ± 0.2) G.] Allowing for the systematic uncertainty in the light intensity, our final result is (2.4 ± 0.5) G per unit imbalance. The gradient given by Eq. (72) with $g_F = 1/4$ (i.e., the value for the $F = 4$ ground state of cesium) is 2.52 G, so our result is close to the theoretical expectation for a $F = 1 \rightarrow 2$ transition in one dimension. This is somewhat surprising, since the trap is three dimensional and the transition involved is $F = 4 \rightarrow 5$. It is possible that the $4 \rightarrow 5$ transition produces a larger force in one dimension, but this is reduced by the three-dimensional geometry.[34] Another possible source of discrepancy with the theory lies in the effect of the repumping light. We observed no significant change in our measurements when the intensity of the repumping light was halved, suggesting that the force exerted by this radiation was not affecting the measurements. However, this test was carried out only at intermediate values of $\Omega^2/\delta\Gamma$ and not at low values, where the trapped cloud was becoming difficult to detect because of its low fluorescent intensity and loading rate. This difficulty limited the range of values of $\Omega^2/\delta\Gamma$ at which the measurements could be made.

Most of our measurements were made on a trap with a

vertical magnetic-field gradient of 16 G/cm, though sometimes smaller gradients were used. The range of imbalance used was $w = -0.3 \rightarrow +0.3$, which is sufficient to move the cloud through a distance several times its diameter. The magnetic field in the cloud was therefore of uniform direction at the extremes of the imbalance values used, and it was these values that fixed the value of field per imbalance ratio, which is plotted in Figs. 7–10. There remains the possibility that the effect of intensity imbalance is different from that indicated by our measurements when the imbalance is sufficiently small that the trapped cloud moves only within its own diameter. We have not yet performed measurements sufficiently accurate to test for this possibility.

D. Further Remarks

We observed a further piece of experimental evidence for the role of polarization gradient forces in the trap. When the intensity imbalance was increased to approximately $w = 0.4$, the trapped cloud changed shape: Instead of moving farther as the imbalance was increased, the brightest region of the cloud stayed at a fixed place, while a fan of atoms extended out into the region of higher magnetic field. As various combinations of vertical and horizontal beams were imbalanced, the fan always spread in the direction of the higher magnetic field. The size of this fan-shaped cloud was several times the size of the cloud at the zero of the magnetic field (i.e., at zero imbalance). The value of imbalance at which the spreading occurred was roughly independent of the magnetic-field gradient, of the position of the cloud in the overlapping laser beams, and of the laser detuning. All of this is what one expects from the induced-orientation theory, as is described in Section 9. The cloud is spreading because it has reached the magnetic field at which the Larmor precession rate is of the order of the light shift; therefore the spring constant of the trap is reduced to that given by the Doppler theory, and the cloud spreads out. Observation of this fanning of the cloud gives a diagnostic that can be used to map a contour of the magnetic field (at ~1 G) around the center of the trap.

Another notable feature is that when the trap is well aligned the quarter-wave plate on either one of the vertical beams can be rotated through 360° without destroying the trap. Alternatively, one can remove the wave plate on one of the retroreflected horizontal beams. The cloud merely becomes somewhat larger and dimmer. We do not have a good understanding of this effect but suggest that the continuing good confinement reflects the insensitivity of the polarization-gradient forces to the light intensity—presumably our wave plates are not perfect, and a small component of light of the correct polarization for confinement is always present.

The theory that was tested by the measurements described above is strictly valid only when the trapped cloud is not optically thick. This condition held, since the measurements were at low saturation and low atomic density ($<10^9$ atoms/cm^3). For completeness we report here that we have also observed collective motion in the trap resulting from reabsorption of photons scattered in the cloud[4] when the laser intensity and the trapped atomic density were increased. A ring surrounding a central ball of atoms was observed when one of the horizontal beams was misaligned by 8 mrad vertically and 3 mrad horizontally; the atoms were loaded from a room-temperature cesium vapor at a pressure of 10^{-9} Torr. We have not made a quantitative study of the collective motion.

10. CONCLUSION

In this paper we have provided an overview of most of the physics of the magneto-optical trap, the main features not discussed being collisions between cold atoms within the trap and the capture process. Our consideration of loss by collisions with fast atoms implies that when the trap is loaded from a laser-cooled atomic beam it is worth shielding it from collisions with fast atoms in the beam. Our consideration of the sub-Doppler theory of the radiation force gave a basic framework with which to understand the magneto-optical trap. The spring constant at the center of the trap is produced by the induced-orientation effect, while the friction parameter is produced by a combination of Sisyphus cooling and induced orientation. The sizes of the force parameters are expected to depend on the relative phase of the trapping beams. For typical operating conditions the maximum atomic density that can be obtained in a magneto-optical trap is limited by photon pressure within the trapped cloud. Our rough estimate of this effect indicates that, by operating the trap at low intensity and high detuning (as long as the loading rate is kept up), one can obtain higher densities than have previously been reported.

Our experimental results confirm the overall picture, but a calculation for the $4 \rightarrow 5$ transition, allowing for the magnetic field and three-dimensional geometry, would be needed to provide a better comparison. With the (three-dimensional) trap operated on the $4 \rightarrow 5$ transition in cesium, our measurements indicate that the magnitude of the confining force, at low saturation, is 1 ± 0.2 times that predicted for the induced-orientation effect on a $1 \rightarrow 2$ transition in a one-dimensional standing wave, where the Lande g value of the lower level is 0.25. Observation of the time for motion to the center of the trap showed that the ratio of frictional to confining forces cannot be understood in terms of induced orientation alone. This damping time indicates that the friction coefficient is of the order of that expected for Sisyphus cooling.

We made accurate measurements of the separation of the interference fringes in the fluorescence from the trap, which are observed when one of the six trapping beams is slightly misaligned. These measurements showed that from one fringe to the next the relative time phase between the misaligned traveling wave and the other waves goes through one complete cycle. We have not given a thorough explanation of this phenomenon, but we have shown that it is caused not by variations in the depth of optical potential (the ac Stark effect) but by more subtle variations in the total light field; the variations have a spatial period equal to the one that we measured.

We have not yet confirmed experimentally our prediction for the maximum possible density in a magneto-optical trap, but our measurement of loss from the trap at low densities gave a collisional cross section in agreement with previous reports, which we have explained in terms of resonant dipole–dipole scattering between excited ce-

sium atoms in the trap and ground-state cesium atoms in the background gas.

REFERENCES AND NOTES

1. E. L. Raab, M. Prentiss, A. Cable, S. Chu, and D. Pritchard, "Trapping of neutral sodium atoms with radiation pressure," Phys. Rev. Lett. **59,** 2631 (1987).
2. S. Chu and C. Wieman, eds., feature on laser cooling and trapping of atoms, J. Opt. Soc. Am. B **6,** 2019–2278 (1989).
3. A. Steane and C. Foot, "Laser Cooling below the Doppler limit in a magneto-optical trap," Europhys. Lett. **14,** 231 (1991).
4. D. Sesko, T. Walker, and C. Wieman, "Behavior of neutral atoms in a spontaneous force trap," J. Opt. Soc. Am. B **8,** 946 (1991).
5. K. Molmer, "Friction and diffusion coefficients for cooling of atoms in laser fields with multidimensional periodicity," Phys. Rev. A **44,** 5820 (1991).
6. N. Wax, *Selected Papers on Noise and Stochastic Processes* (Dover, New York, 1954), Eq. (297), p. 40.
7. J. Nellessen, J. Werner, and W. Ertmer, "Magneto-optical compression of a monoenergetic sodium atomic beam," Opt. Commun. **78,** 300 (1990).
8. D. Sesko, T. Walker, C. Monroe, A. Gallagher, and C. Wieman, "Collisional losses from a light-force atom trap," Phys. Rev. Lett. **63,** 961 (1989).
9. C. Monroe, W. Swann, H. Robinson, and C. Wieman, "Very cold trapped atoms in a vapor cell," Phys. Rev. Lett. **65,** 1571 (1990).
10. H. Metcalf, "Magneto-optical trapping and its application to helium metastables," J. Opt. Soc. Am. B **6,** 2206 (1989).
11. E. A. Power, *Introductory Quantum Electronics* (American Elsevier, New York, 1965).
12. M. Prentiss, A. Cable, J. E. Bjorkholm, S. Chu, E. L. Raab, and D. Pritchard, "Atomic-density-dependent losses in an optical trap," Opt. Lett. **13,** 452 (1988).
13. A. Cable, M. Prentiss, and N. P. Bigelow, "Observations of sodium atoms in a magnetic molasses trap loaded by a continuous uncooled source," Opt. Lett. **15,** 507 (1990).
14. E. L. Raab, "Trapping sodium with light," Ph.D. dissertation (Massachusetts Institute of Technology, Cambridge, Mass., 1988).
15. P. Julienne and F. Mies, "Collisions of ultracold trapped atoms," J. Opt. Soc. Am. B **6,** 2257 (1989).
16. H. S. W. Massey, *Electronic and Ionic Impact Phenomena* (Oxford U. Press, London, 1971), Vol. 3.
17. A. Corney, *Atomic and Laser Spectroscopy* (Oxford U. Press, London, 1977), Chap. 8.
18. T. Walker, D. Sesko, and C. Wieman, "Collective behavior of optically trapped neutral atoms," Phys. Rev. Lett. **64,** 408 (1990).
19. J. Dalibard, "Laser cooling of an optically thick gas: the simplest radiation pressure trap?" Opt. Commun. **68,** 203 (1988).
20. R. Loudon, *The Quantum Theory of Light* (Oxford U. Press, London, 1983), Chap. 8.
21. B. Mollow, "Power spectrum of light scattered by two-level systems," Phys. Rev. **188,** 1969 (1969).
22. B. Mollow, "Stimulated emission and absorption near resonance for driven systems," Phys. Rev. A **5,** 2217 (1972).
23. W. Phillips and H. Metcalf, "Laser deceleration of an atomic beam," Phys. Rev. Lett. **48,** 596 (1982).
24. P. Lett, W. Phillips, S. Rolston, C. Tanner, R. Watts, and C. Westbrook, "Optical molasses," J. Opt. Soc. Am. B **6,** 2084 (1989).
25. E. Riis, D. Weiss, K. Moler, and S. Chu, "Atom funnel for the production of a slow, high-density atomic beam," Phys. Rev. Lett. **64,** 1658 (1990).
26. J. Dalibard and C. Cohen-Tannoudji, "Laser cooling below the Doppler limit by polarization gradients: simple theoretical models," J. Opt. Soc. Am. B **6,** 2023 (1989).
27. B. Sheehy, S.-Q. Shang, P. van der Straten, S. Hatamian, and H. Metcalf, "Magnetic-field induced laser cooling below the Doppler limit," Phys. Rev. Lett. **64,** 858 (1990).
28. S.-Q. Shang, B. Sheehy, P. van der Straten, and H. Metcalf, "Velocity-selective magnetic resonance laser cooling," Phys. Rev. Lett. **65,** 317 (1990).
29. S.-Q. Shang, B. Sheehy, and H. Metcalf, "Velocity-selective resonances and sub-Doppler laser cooling," Phys. Rev. Lett. **67,** 1094 (1991).
30. We use this expression following Refs. 28 and 29, although the name is slightly misleading, since there is no oscillating magnetic field: The mathematical description is merely analagous to a magnetic resonance.
31. A. Hemmerich, D. Schropp, and T. Hänsch, "Light forces in two crossed standing waves with controlled time phase difference," Phys. Rev. A **44,** 1910 (1991).
32. N. Bigelow and M. Prentiss, "Observation of channeling of atoms in the three-dimensional interference pattern of optical standing waves," Phys. Rev. Lett. **65,** 29 (1990).
33. N. Bigelow and M. Prentiss, "Decreased damping of ultracold atoms in optical molasses: predictions and a possible solution," Opt. Lett. **15,** 1479 (1990).
34. G. Nienhuis, P. van der Straten, and S.-Q. Shang, "Operator description of laser cooling below the Doppler limit," Phys. Rev. A **44,** 462 (1991); A. Steane, G. Hillenbrand, and C. Foot, "Polarization gradient cooling in a one-dimensional σ^+–σ^- configuration for any atomic transition," J. Phys. B (to be published).
35. T. Bergman, G. Erez, and H. Metcalf, "Magnetostatic trapping fields for neutral atoms," Phys. Rev. A **35,** 1535 (1987). N. B.: There is an error in Table II. B_ρ for $n = 3$ is missing a z and should read $-3\rho z^2/2 + 3\rho^2 z/8$.
36. C. Wieman and L. Hollberg, "Using diode lasers for atomic physics," Rev. Sci. Instrum. **62,** 1 (1991).
37. "Pressure measurement and electron beam guns," in *Vacuum Generators Product Manual* (Vacuum Generators Ltd., Hastings, UK, 1991), Sec. 07; S. Dushman, *Scientific Foundations of Vacuum Technique* (Wiley, New York, 1949).
38. C. Salomon, J. Dalibard, W. D. Phillips, A. Clairon, and S. Guellati, "Laser cooling of cesium atoms below 3 μK," Europhys. Lett. **12,** 683 (1990).